



Title	Self-adaptive formation of uneven node spacings in wild bamboo
Author(s)	Shima, Hiroyuki; Sato, Motohiro; Inoue, Akio
Citation	Physical review E, 93(2), 022406-1-022406-9 https://doi.org/10.1103/PhysRevE.93.022406
Issue Date	2016-02-10
Doc URL	http://hdl.handle.net/2115/60843
Rights	©2016 American Physical Society
Type	article
File Information	PhysRevE.93.022406.pdf



[Instructions for use](#)



Self-adaptive formation of uneven node spacings in wild bamboo

Hiroyuki Shima*

Department of Environmental Sciences, University of Yamanashi, 4-4-37 Takeda, Kofu, Yamanashi 400-8510, Japan

Motohiro Sato

Division of Engineering and Policy for Sustainable Environment, Faculty of Engineering, Hokkaido University, Kita-13, Nishi-8, Kita-ku, Sapporo, Hokkaido 060-8628, Japan

Akio Inoue

Faculty of Environmental and Symbiotic Sciences, Prefectural University of Kumamoto, 3-1-100 Tsukide, Higashi-ku, Kumamoto, Kumamoto 862-8502, Japan

(Received 24 September 2015; revised manuscript received 2 January 2016; published 10 February 2016)

Bamboo has a distinctive structure wherein a long cavity inside a cylindrical woody section is divided into many chambers by stiff diaphragms. The diaphragms are inserted at nodes and thought to serve as ring stiffeners for bamboo culms against the external load; if this is the case, the separation between adjacent nodes should be configured optimally in order to enhance the mechanical stability of the culms. Here, we reveal the hitherto unknown blueprint of the optimal node spacings used in the growth of wild bamboo. Measurement data analysis together with theoretical formulations suggest that wild bamboos effectively control their node spacings as well as other geometric parameters in accord with the lightweight and high-strength design concept.

DOI: [10.1103/PhysRevE.93.022406](https://doi.org/10.1103/PhysRevE.93.022406)

I. INTRODUCTION

Bamboo is a fascinating tropical plant native to East and Southeast Asia. A salient feature of bamboo is its growth rate: the fastest among all the world's woody plants [1]. Several species of bamboo grow 1 m per day, with no need for fertilizers or watering. The rapid maturity of bamboo groves affords them a clear advantage for survival over competing tree species, yielding low-cost and easily available materials that can be used in the construction and pulp industries [2–5]. Moreover, a significant capability of bamboo for biomass accumulation has been suggested in the past [6–8], especially for carbon storage, which is beneficial to the global carbon cycle [9–11]. With these ecofriendly properties, bamboo has cropped up as a green alternative to other woody raw materials [5].

From a mechanical standpoint, bamboo can be considered a nature-derived smart material in which a high stiffness and light weight coexist [3,12–14]. Its stiffness against tensile loading is due to the longitudinal arrays of cellulose fibers embedded within a ligneous matrix [15,16]. The volume fraction of the fibers is maximum at the outer surface of the culm wall and decreases monotonically in the inward direction [17]. This gradient distribution of fibers is effective in reinforcing the whole bamboo in a similar manner as functionally graded composite materials [18–23]. Another important feature of bamboo, its light weight, is a direct consequence of its hollow and cylindrical structure. Hollowness is in general preferred for carrying loads compared with solid counterparts of the same cross-sectional area [24]. In addition, hollow cylinders use less material and are lighter while resisting the same bending or torsional loads.

One possible disadvantage caused by hollowness is ease of collapse when a strong bending force is applied. In order

to overcome this limitation, bamboos form many “nodes” at intervals along the culm (see Fig. 1). A node is a combination of an external ridge at the outer surface and an internal diaphragm embedded in the hollow cavity (Fig. 2). Since a diaphragm acts as a ring stiffener for the region near the node, sequential insertion of many diaphragms with an appropriate spacing leads to improvement in the mechanical stiffness of the whole bamboo culm [19,25–30]. However, this argument poses a question: What node spacings are optimal for adapting to bending damage caused by external forces?

Obviously, the stability of the culm under bending is enhanced by installing diaphragms as densely as possible. However, the excessive density of diaphragms makes the whole culm heavier and inhibits the growth rate of bamboo. It is expected, therefore, that there is an optimum configuration of node spacings that bamboos have acquired inherently after millions of years of evolution. Taking a closer look, in fact, one may find that the spacing between adjacent nodes (i.e., the internode length) is not constant but, rather, is longest slightly below the middle part of the culm and gradually diminishes from there toward the ends of the culm (see Refs. [31] and [32], for instance). The purpose of this article is to elucidate the origin of inhomogeneity in internode lengths in wild bamboo using the language of structural mechanics. Combining theoretical results with experimental bamboo geometry data, we demonstrate that the inhomogeneity of internode lengths is a consequence of the self-adaptive property of wild bamboo for securing mechanical stability against bending.

II. MECHANICS OF HOLLOW CYLINDERS

A. Ovalization under pure bending

A bamboo culm is an orthotropic hollow cylinder divided into chambers by stiff diaphragms positioned at the nodes. Heterogeneity and anisotropy in the internal microstructure of the woody portion may contribute to the mechanical superiority of

*hshima@yamanashi.ac.jp



FIG. 1. Left: Wild bamboo grove. Right: Notation and terminology specifying each segment of a whole bamboo “culm.” The stem of bamboo is technically known as a culm since bamboo is the vernacular or common term for members of a particular taxonomic group of large woody grasses (family Poaceae) [8].

bamboo culms. To make a concise argument, nevertheless, we use a simplified theoretical model to formulate the mechanics of a bamboo culm under bending.

Our primary hypothesis is that a bamboo culm is a long, straight, thin-walled cylinder made from a homogeneous and elastic material. The study of the mechanical stability of elastic cylinders has a long history [33–36] and is well established for the case of hollow cylinders with circular cross sections. When the cylinder is bent uniformly, the longitudinal tension and compression that resist the applied bending moment tend to flatten the cross section [33] as sketched in Fig. 3. The gradual change in the cross section leads to a reduction in the bending stiffness of the cylinder with increasing applied moment. After the bending moment reaches a maximum value, the structure become unstable and so the object suddenly forms a kink [37].

The initial bending behavior of the cylinder is characterized by a uniform ovalization of the cross section [38,39]. In the unloaded state, the cylinder’s axis is straight and its cross section is perfectly circular. However, if a small moment is applied, the axis attains a constant curvature and ovalizes. The degree of ovalization is quantified by the dimensionless parameter ζ , called the oblateness. Given an initially circular cross section of radius r , the product $r\zeta$ is equal to the reduction in the minor radius of the oval obtained after deformation.

For later use, we introduce another dimensionless parameter, Γ , by considering the curvature of the cross-sectional curve. An illustrative diagram is given in Fig. 4. In general, the curvature of the cross-sectional curve is written $d\psi/ds$. Here, ψ is the angle between the tangent at a point on the



FIG. 2. Left: Segment of a bamboo culm. Right: Magnified view of the section near a diaphragm.

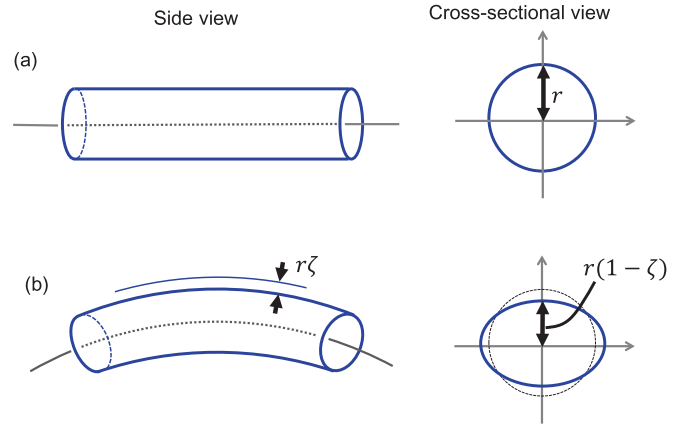


FIG. 3. Side and cross-sectional views of an elastic hollow cylinder. (a) A straight cylinder before bending. (b) A deformed cylinder after bending. The degree of ovalization in the cross section is quantified by the dimensionless parameter ζ , called the oblateness.

curve and the vertical line (i.e., the y axis); s is the arc length measured from the x axis to the point. Assuming that the cross-sectional deformation is small and inextensional in the circumferential direction, we have

$$\frac{d\psi}{ds} = \frac{1}{r} + \frac{3\Gamma}{r} \cos \frac{2s}{r}. \tag{1}$$

Here, the first term on the right-hand side is the original curvature, and the second term represents the change in the curve’s curvature obtained after ovalization. We see later that Γ serves as a basic variable for the strain energy of the thin-walled cylinder under bending.

The relation between Γ and our oblateness ζ is deduced from the argument below. Equation (1) implies that $\psi = (s/r) + (3\Gamma/2) \sin(2s/r)$. We also have $dy = \cos \psi ds$ by elementary trigonometry. Combining the two results, it is possible to prove that

$$y(s) = \int_0^s \cos \left(\frac{\tilde{s}}{r} + \frac{3\Gamma}{2} \sin \frac{2\tilde{s}}{r} \right) d\tilde{s}. \tag{2}$$

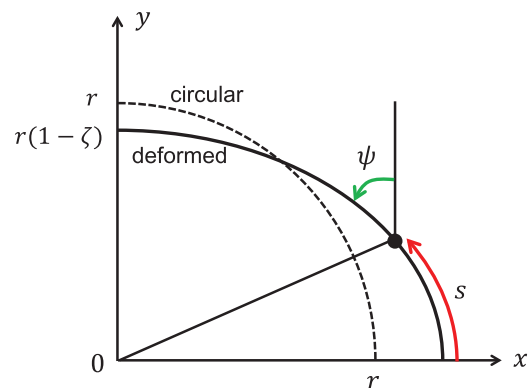


FIG. 4. Coordinate system used for analysis of ovalization under bending. A quarter round of the cross section is depicted in the x - y plane.

For relatively small Γ , the Taylor-series expansion is applied to the integrand in Eq. (2) to obtain

$$\begin{aligned} \frac{y(s)}{r} = & \sigma - \Gamma\sigma^3 - \Gamma^2\left(\frac{3}{2}\sigma^3 - \frac{9}{10}\sigma^5\right) \\ & + \Gamma^3\left(\frac{9}{10}\sigma^5 - \frac{9}{14}\sigma^7\right) + \dots, \end{aligned} \quad (3)$$

where $\sigma \equiv \sin(s/r)$. Specifically, at the apex characterized by $\sigma = 1$, we have $y = r(1 - \zeta)$, with ζ being oblateness. Therefore, it follows that ζ and Γ are interdependent through the relation

$$\zeta = \Gamma + \frac{3}{5}\Gamma^2 - \frac{9}{35}\Gamma^3 + \dots \quad (4)$$

Equation (4) means that Γ is nearly equal to ζ if ovalization is sufficiently slight so that $\Gamma \ll 1$.

B. Strain energy of deformed cylinders

We are in a position to formulate the strain energy of bamboo culms under pure bending. We first remember that bamboo is an anisotropic material owing to its structure, which is a lignin matrix reinforced with fibers aligned in the longitudinal direction of the culm. These fibers provide a higher stiffness and strength along the axial direction compared to those along the transverse axis. As a result, the Young's modulus parallel to the cylinder axis, designated E_{\parallel} , differs from that in the circumferential direction, E_{\perp} . In typical bamboos, the ratio E_{\parallel}/E_{\perp} has been estimated to be a few tens or less [19,21,23,40–42]. Bearing this anisotropy in mind, we formulate the total strain energy per unit length, U , of a cylinder whose centroidal axis has been deformed into an arc of curvature κ [38]:

$$U = F_{\parallel}(\kappa, \Gamma(\kappa)) + F_{\perp}(\Gamma(\kappa)), \quad (5)$$

$$\begin{aligned} F_{\parallel}(\kappa, \Gamma(\kappa)) = & \frac{\pi E_{\parallel}}{2} \cdot r^3 w \kappa^2 \\ & \times \left\{ 1 - \frac{3}{2}\Gamma(\kappa) - \frac{1}{2}\Gamma(\kappa)^2 + \frac{21}{16}\Gamma(\kappa)^3 \right\}, \end{aligned} \quad (6)$$

$$F_{\perp}(\Gamma(\kappa)) = \frac{3\pi E_{\perp}}{8} \cdot \frac{w^3}{r} \Gamma(\kappa)^2. \quad (7)$$

Here, w is the wall thickness, and the notation $\Gamma(\kappa)$ indicates explicitly that Γ is a function of κ . In the above expressions, F_{\parallel} accounts for the strain energy of longitudinal stretching, and F_{\perp} represents the strain energy of circumferential bending.

Note that F_{\perp} is simply a parabolic function of Γ with no higher order terms. This is because F_{\perp} is determined by the ovalization-induced change in the curvature of the cross-sectional curve, which is directly proportional to Γ [see Eq. (1)]. On the other hand, F_{\parallel} involves higher order terms with respect to Γ , since it is determined by the second moment of area of the deformed cross section, which is proportional to $\int_0^{\pi r/2} y^2 ds$. Using the expansion of Eq. (3), the second moment of area is written by a power series in Γ . In our computation, the terms up to the order of Γ^3 have been taken into account to obtain the expression of Eq. (6).

Given a value of κ , the optimum value of Γ (and that of ζ) is determined by the equilibrium condition of $\partial U / \partial \Gamma = 0$.

It follows from Eqs. (5)–(7) that at the equilibrium state, Γ should satisfy

$$\frac{E_{\parallel}}{E_{\perp}} \cdot \frac{r^4}{w^2} \kappa^2 \left(\frac{1}{\Gamma} + \frac{2}{3} - \frac{63}{24}\Gamma \right) = 1. \quad (8)$$

Therefore, by solving Eq. (8) with respect to Γ and substituting the solution into Eqs. (5)–(7), we can write U as a function of κ alone. We then numerically calculate the bending moment, $m = dU/d\kappa$, and its dependence on κ . The results indicate that m reaches a maximum at a curvature of

$$\kappa = \left(\frac{E_{\perp}}{E_{\parallel}} \right)^{\frac{1}{2}} \frac{w}{r^2} \times 0.485, \quad (9)$$

which corresponds to $\Gamma = 0.235$ and the oblateness of

$$\zeta = 0.268 \simeq \frac{4}{15}. \quad (10)$$

Interestingly, the characteristic value of ζ given by Eq. (10) is independent of any of the parameters defining the cylinder's elasticity and geometry [33]. In other words, the maximum of m is reached when the shorter radius of the ovalized cross section becomes equal to approximately 73% of the radius of the original circular cross section, regardless of the elastic constants, initial circular radius, and wall thickness of the cylinder. If we apply a bending moment that exceeds the maximum, ζ goes beyond the value in Eq. (10) and the cylinder will collapse owing to loss of mechanical resilience against deformation.

C. Cap-induced stiffening

Our previous discussion has been pertinent to sufficiently long cylinders under the open-ended condition; i.e., those with no cap at the two ends. If the cylinder is relatively short and rigid circular caps are fixed at both ends of the cylinder, then the ovalization can be largely suppressed as a whole because of the boundary condition that the cross sections at the two ends keep their original circular shapes. This ‘‘held-circular’’ effect at the edges propagates in the axial direction from the edges to the middle of the cylinder; therefore, the closer a cross section is to either of the two ends, the more the ovalization at the cross section is suppressed.

It is understood intuitively that the efficiency of cap-induced suppression of ovalization depends on the cylinder length ℓ , cylinder radius r , and wall thickness w . In the following discussion, we demonstrate how to quantify the efficiency of suppression in terms of geometric parameters such as ℓ , r , and w .

Figure 5(a) shows the curved profile of a portion of an open-ended, long, hollow cylinder which has been subjected to a pure bending moment. The applied bending moment corresponds to a certain value of ζ no more than 4/15. The amount of ovalization in the cross section is constant over the whole cylinder, including the two ends. This spatial uniformity in oblateness is broken if we attach caps at the two ends. The held-circular effect driven by the caps is schematically illustrated in Fig. 5(b); since the ends preserve the original circular shape, there are likely to be transition zones in the vicinity of the two ends, within which ζ increases from 0 at the ends to the given value over a central region.

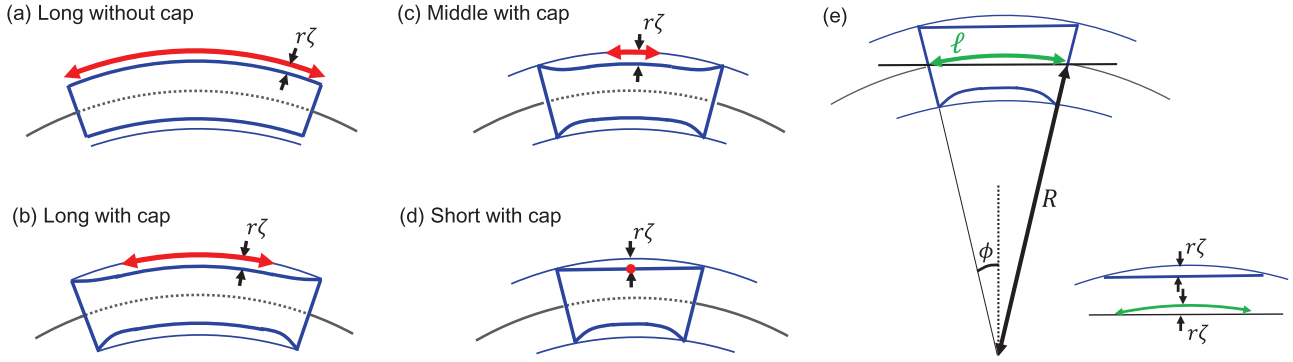


FIG. 5. (a) Curved profile of a portion of an open-ended, long, hollow cylinder. (b) A closed-ended long cylinder. (c) A closed-ended medium-length cylinder. (d) A closed-ended short cylinder. (e) The relationship between the curvature radius R and the cylinder length ℓ under the conditions in (d).

It is obvious that, for cylinders which are shorter than the one depicted in Fig. 5(b), the central region in which ζ remains effectively constant is also shorter; see Fig. 5(c). Indeed, for even shorter cylinders, the held-circular effect may well dominate behavior over the entire length of the cylinder. In Fig. 5(d), a cylinder has been sketched which is so short that the generator on the outer side remains approximately straight. This suggests that a cylinder having this geometry should fall in the range over which the held-circular effect is dominant.

Special attention is paid to the case in which the central zone shrinks to a point on the generator, as depicted in Fig. 5(d). In this extreme situation, the oblateness at the central point and the curvature of the cylindrical axis, designated ζ^* and κ^* , respectively, satisfy the relation

$$\kappa^* = \frac{8r\zeta^*}{\ell^2}, \quad (11)$$

as accounted for in Fig. 5(e) (the mathematical derivation is given in Appendix A.) We also note that κ^* and ζ^* are interdependent through the same relation as in Eq. (8). Eliminating κ^* from the relation and using Eq. (11), we obtain

$$64\zeta^* \cdot \frac{E_{\parallel}}{E_{\perp}} \cdot \frac{r^6}{\ell^4 w^2} = 1. \quad (12)$$

Let us introduce a dimensionless parameter:

$$\Omega \equiv \left(\frac{E_{\perp}}{E_{\parallel}} \right)^{\frac{1}{4}} \cdot \left(\frac{\ell^2 w}{r^3} \right)^{\frac{1}{2}}. \quad (13)$$

Equation (12) is then simplified as

$$\zeta^* = \frac{\Omega^4}{64}. \quad (14)$$

Recall that, for open-ended long cylinders, ζ has an upper limit for maintaining structural stability; a ζ larger than $4/15$ leads to collapse of the cylinder under bending. This holds true even for closed-ended short cylinders; if ζ^* is found to exceed $4/15$ under a steadily increasing bending moment, the cylinder has already been collapsed before the central region (that is, the ζ -constant region) shrinks to a point. In this case, the caps that were installed at the two edges make only a minor contribution as stiffeners. In contrast, if ζ^* is kept less than $4/15$, then ζ at an arbitrary section underruns the threshold because of the

held-circular effect. In other words, when

$$\Omega < \left(\frac{256}{15} \right)^{\frac{1}{4}} \simeq 2.033, \quad (15)$$

the held-circular effect dominates over the whole cylinder so that $\zeta < 4/15$ is guaranteed at an arbitrary section. It is seen from Eq. (12) that a small ℓ and large r are preferred in order for the inequality of Eq. (15) to be satisfied.

III. Ω PROFILE IN WILD BAMBOO

A. Towards the optimal Ω distribution

We have argued that the diaphragms in bamboos give rise to the held-circular effect on every short culm segment sandwiched between adjacent nodes. It is inferred, therefore, that the number of diaphragms inserted is regulated by a balance between the lightweight property obtained by extending the internode lengths and the mechanical stability achieved by reducing the internode lengths. The latter requirement is attributed to Eq. (13), which indicates that a small ℓ leads to a small Ω , thus suppressing the deformation of culm segments between nodes under bending.

The story does not end here. Typically, the nodes are sparsely distributed at the middle height and densely distributed near the top and bottom of the bamboo. So, what mechanism leads to these inhomogeneous internode lengths?

At first glance, the dense population of nodes near the tip might appear to cause significant reinforcement at the apical part of a bamboo culm. Similarly, the sparse population of nodes at the middle height may seem to imply the nonnecessity of reinforcement there. These two speculations are, nonetheless, totally irrelevant. What we should pay attention to is not the population density of nodes but the spatial variation of Ω along the culm. Since Ω is a function of several geometric parameters such as w , r , and ℓ , the optimal distribution in Ω is expected to regulate those parameters; as a result, ℓ becomes small (or large) at the tip (middle height) of bamboo culms, although there is seldom (significant) need for reinforcement there. We prove in the following discussion that this idea is supported by measurement data analysis for moso bamboos (i.e., *Phyllostachys pubescens*), which are one of the best-known and largest-scale species of natural bamboos in Japan [9]. In the remainder of this section, we try to formulate

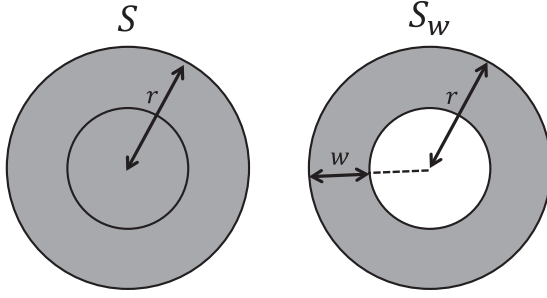


FIG. 6. Cross-sectional view of a bamboo culm with radius r and wall thickness w . S represents the cross-sectional area surrounded by the outer surface, and S_w is the cross-sectional area of the woody part (excluding the hollow cavity).

a universal law for Ω as a function of the elevation from the ground.

B. Wall thickness w

Consider that we have many native-grown bamboos with various geometric quantities (w , r , and ℓ) as well as a total culm height H . Among the quantities, w and r are known to obey a simple proportional law. It was found in Ref. [43] that for moso bamboos, the cross-sectional area of the whole culm S and that of the culm wall S_w are related by (see Fig. 6)

$$\frac{S - S_w}{S} = \varepsilon, \quad (16)$$

with a constant ε . Since $S = \pi r^2$ and $S_w = S - \pi(r - w)^2$, Eq. (16) is rewritten as

$$\frac{w}{r} = 1 - \sqrt{\varepsilon}. \quad (17)$$

Note that the proportional law of Eq. (17) holds for cross sections at arbitrary height. Substituting this into Eq. (13), the expression of Ω can be simplified as

$$\Omega = \frac{\ell}{r} \cdot \left(\frac{E_{\perp}}{E_{\parallel}} \right)^{\frac{1}{4}} (1 - \sqrt{\varepsilon})^{\frac{1}{2}}. \quad (18)$$

The appropriate values of E_{\perp}/E_{\parallel} and ε for moso bamboos are listed in Table I.

C. Culm radius r

The second central hypothesis of our analysis is that every bamboo has the shape of a circular, truncated cone with an

TABLE I. List of parameters.

a	1.096
b	0.871
ε	0.689
$1 - \sqrt{\varepsilon}$	0.170
η	7.216
E_{\perp}/E_{\parallel}	1/16
c_1	-1.430
c_2	1.834
c_3	0.596

extremely high aspect ratio. The generator of the cone is not exactly straight but rather is slightly convex outward. The cylindrical symmetry of the hypothesized shape allows us to write the radius r of a given bamboo culm at a certain height h as

$$r = f(h) \quad \text{with} \quad 0 \leq h \leq H,$$

where $h = 0$ at the base of the bamboo and $h = H$ at the tip. The functional form of $f(h)$ is sample dependent in principle, which indicates the absence of a one-to-one relation between r and h that is universal to every samples. Nevertheless, an appropriate normalization procedure makes it possible to construct a universal law for the geometry of native-grown bamboos. A broadly accepted form of this law is the so-called Kunze's curve [44], which reads [45–47]

$$\frac{r}{r_{0.1}} = a \left(1 - \frac{h}{H} \right)^b, \quad (19)$$

with constants a and b . In Eq. (19), we have introduced the notation $r_{\alpha} \equiv f(\alpha H)$ with $\alpha = 0, 0.1, 0.2, \dots, 0.9, 1$. Hence, $r_{0.1}$ represents the radius of bamboo at the relative height of 10% from the base. Equation (19) indicates that normalized profiles of bamboos are governed by only the two parameters a and b , whose values are dependent on the bamboo species, as explained later.

Figure 7 illustrates the normalization procedure we have mentioned. It is clear from Fig. 7(b) that Kunze's curve intersects the point $(h/H, r/r_{0.1}) = (0.1, 1)$. Substituting these coordinates into Eq. (19), we obtain $a = (10/9)^b$. The value of b (and thus of a , as well) for moso bamboo was evaluated based on a statistical argument over many samples, as explained later.

D. Internode length ℓ

The final hypothesis of our study regards the spatial distribution of ℓ along the whole culm. To proceed, we define the label n for a sequence of internodes in bamboo. The undermost internode that appears immediately aboveground is assigned $n = 1$, and the uppermost internode at the tip is assigned $n = N$. Here, N is the total number of internodes contained in a given bamboo culm. Obviously, the value of N is strongly sample dependent because of the variation in culm sizes. To eliminate the influence of size variation, we normalize n and ℓ by N and $\ell_{\text{av}} \equiv H/N$, respectively. In a similar way, we consider the normalized height of an internode, expressed by h/H . When $N \gg 1$, the variable $x \equiv n/N$ can be regarded as continuous, ranging from 0 (at the base) to 1 (at the tip). Furthermore, the normalized quantities of h/H and ℓ/ℓ_{av} can be considered functions of x . It was indeed found in Ref. [32] that the measurement data for h are well fit by a third-order polynomial with respect to x as

$$\frac{h(x)}{H} = \sum_{k=1}^3 c_k x^k \equiv P_3(x). \quad (20)$$

The estimated values of the coefficients c_k ($k = 1, 2, 3$) for moso bamboo are listed in Table I. It also follows

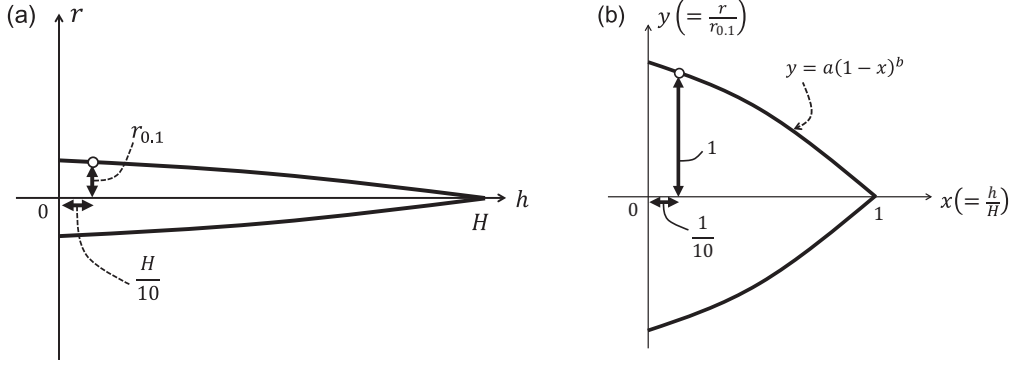


FIG. 7. (a) Kunze's curve in the r - h plane. (b) Normalized counterpart in the x - y plane; the curve necessarily intersects the point $(x, y) = (\frac{1}{10}, 1)$, by its definition.

that

$$\begin{aligned} \ell\left(\frac{n}{N}\right) &= h\left(\frac{n+1}{N}\right) - h\left(\frac{n}{N}\right) \\ &= \frac{h\left(\frac{n+1}{N}\right) - h\left(\frac{n}{N}\right)}{\frac{1}{N}} \times \frac{1}{N}. \end{aligned} \quad (21)$$

As a result, we have, approximately,

$$\ell(x) = \frac{\ell_{\text{av}}}{H} \cdot \frac{h(x + \Delta x) - h(x)}{\Delta x} \simeq \ell_{\text{av}} P_3(x)', \quad (22)$$

where the prime indicates a derivative with respect to x . Reflecting the results of Eqs. (19), (20), and (22) in (18), we finally obtain the spatial distribution of Ω ,

$$\Omega(x) = \eta \left(\frac{E_{\perp}}{E_{\parallel}}\right)^{\frac{1}{4}} \cdot \frac{(1 - \sqrt{\varepsilon})^{\frac{1}{2}}}{a} \cdot \frac{P_3(x)'}{[1 - P_3(x)]^b}, \quad (23)$$

with a constant,

$$\eta = \frac{\ell_{\text{av}}}{r_{0.1}}. \quad (24)$$

Equation (23) provides a unified expression of $\Omega(x)$ that applies to various samples of moso bamboos regardless of their heights and culm radii. We see later that, in wild bamboos, the profile of $\Omega(x)$ is optimized through a combination of a power-law decrease in $r(x) \propto (1-x)^b$ and parabolic behavior of $\ell(x) \propto P_3(x)'$ with increasing x .

IV. RESULTS AND DISCUSSION

A. Setting parameters

Table I summarizes the parameters that characterize the geometry of moso bamboos. They are partly cited from existing measurement data; the values of a and b were reported in Ref. [45], and that of ε was given in Ref. [43]. The value of η has been newly deduced from our database; the method of derivation is described in detail in Appendix B. For numerical consistency, all the parameters in Table I are accurate to the three decimal point (except for E_{\perp}/E_{\parallel}).

B. Fitting curves: $h(x)$ and $\ell(x)$

Figure 8(a) shows a third-degree polynomial curve $P_3(x)$ that fits the experimental data of $h(x)/H$; see Eq. (20).

The values of expansion coefficients c_k with $k = 1, 2, 3$ were obtained by a numerical fitting of the experimental data for $h(x)$ over 50 samples of moso bamboos. In the fitting, we imposed the supplementary condition that $c_1 = 1 - c_3 - c_2$ to comply with the natural assumption that the curve should pass through the two points $(0, 0)$ and $(1, 1)$. The plot in Fig. 8(a) clearly indicates that all the data points fall into a single curve, implying the existence of a universal rule for the internode length in wild moso bamboo.

Figure 8(b) displays a parabolic curve of $\ell(x)/\ell_{\text{av}}$ obtained by differentiation of $P_3(x)$ with respect to x . The Kunze's curve of $r(x)/r_{0.1}$ is also presented for comparison. The curve of $\ell(x)/\ell_{\text{av}}$ shows upward convex behavior, having a maximum at $x \simeq 0.43$, which is located immediately below the exact middle height of the whole culm. These observations are in good agreement with previous studies [31, 32].

It should be remarked that in Fig. 8(b), $\ell(x)$ shows a rapid decrease at large x and eventually converges to 0 at $x = 1$. This means that nodes are populated much more densely near the tip of bamboo culms, far more than near the base ($x = 0$), at which $\ell(x)$ remains ca. 60% of ℓ_{av} . The shrinkage of $\ell(x)$ at the tip may lead us to the misconception that the culm near the tip is substantially stiffened by a considerable number of diaphragms. This wrong idea is resolved upon looking into the spatial variation in Ω that is demonstrated below.

C. Spatial variation in $\Omega(x)$

Figure 8(c) shows the numerical results of $\Omega(x)$ that have been deduced by substituting the fitting function $P_3(x)$ into Eq. (23). The curve of $\Omega(x)$ for $x \leq 0.7$ is presented. It shows a monotonic increase with x , starting from $\Omega \simeq 0.86$ at $x = 0$ to $\Omega \simeq 2.0$ at $x = 0.2$ and beyond. The inset shows the whole curve of $\Omega(x)$, in which an almost-divergent Ω close to $x = 1$ is found.

The most striking observation in Fig. 8(c) is that the criterion of $\Omega < 2.033$ holds for every $x < 0.22$; see Eq. (15). We have specifically found that even at $x \sim 0.22$, the diaphragms remain active for reinforcement. This finding may be counterintuitive for some readers; since $\ell(x) > \ell_{\text{av}}$ at $x \sim 0.22$, one might feel that the diaphragms at the middle height do not work any longer as ring stiffeners but allow flexible deformation of internodes to counter crosswind. Our results evidence that the bend-induced ovalization at the

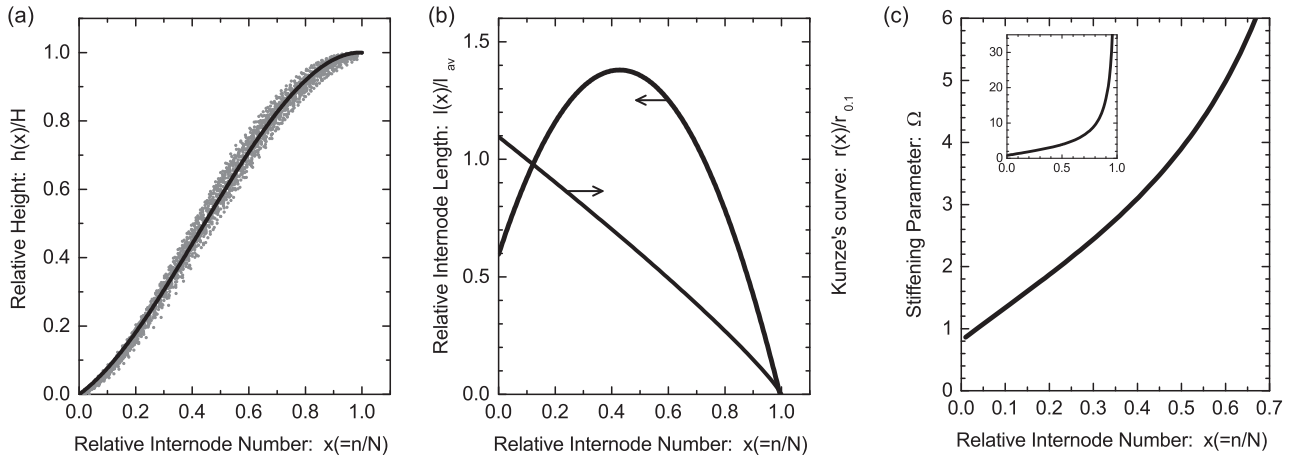


FIG. 8. (a) A third-degree polynomial curve with respect to $x = n/N$ that fits the experimental data on the normalized internode height $h(x)/H$. (b) A parabolic curve expressing the normalized internode length $\ell(x)/\ell_{av}$ as a function of x . The normalized Kunze's curve $r(x)/r_{0.1}$ is also shown. (c) The curve of $\Omega(x)$ within a limited range of x , indicating that the criterion $\Omega < 2.033$ holds for $x < 0.59$. Inset: The whole curve of $\Omega(x)$ over $0 < x < 1$.

middle height is surely suppressed despite the large separation between nodes.

Figure 8(c) also tells us that the effectiveness of reinforcement is greatly enhanced near the base, where Ω becomes less than 1.0. The considerable reduction in Ω is quite reasonable, since bamboo segments near the base are subjected to severe external loading. Figure 9 presents a diagram of the bending moment that is exerted to the bamboo culms under horizontal loading. When the external load P is concentrated at the tip, the magnitude of the applied bending moment increases linearly from the tip to the base as depicted in Fig. 9(a). On the other hand, if the load is uniformly scattered over the whole culm, the applied bending moment shows a parabolic increase [Fig. 9(b)]. In both situations, the bending moment commonly obeys a monotonic variation, having a maximum at the base. Although the load exerted on real wild bamboos will show a more complex dependence on elevation, in general

the maximum bending moment arises at the base. This is the reason why $\Omega(x)$ is required to be considerably small near $x = 0$.

Further attention should be paid to the qualitative agreement in the profile between the $\Omega(x)$ curve [Fig. 8(c)] and the diagram of the bending moment [Fig. 9]. We have seen that the applied bending moment decreases monotonically from the base to the tip, which implies that the need for reinforcement becomes lower as the altitude increases. Correspondingly, $\Omega(x)$ shows a monotonically increasing curve with x , meaning that the degree of reinforcement disappears gradually toward the tip. This coordinated monotonicity in the $\Omega(x)$ curve and the bending moment diagram indicates a plausible guiding principle of wild bamboo's morphology. Namely, in the growing process, bamboos control their geometric parameters such as $\ell(x)$, $r(x)$, and $w(x)$ so that the resulting $\Omega(x)$ increases with x in a monotonic manner. In this context, the node-induced reinforcement of the culm should be almost unnecessary near the tip; it is inferred, therefore, that diaphragms near the tip serve only to support the weight of branches and leaves that are densely distributed around the tip [48]. In fact, it is widely observed that bamboo typically produces new shooting branches from the nodes positioned higher than the middle part of the culm. In addition, each new branch grows upwards from the node and grows leaves. These imply a role for the nodes near the tip in sustaining the branches, instead of reinforcing the culm.

We emphasize that an assessment of the spatial variation of $\Omega(x)$ is crucially important to gaining insight into the role of nodes and internodes in bamboo mechanics. A simple observation of $\ell(x)$ alone is of no use; in reality, the combination of spatial variation in $\ell(x)$, $r(x)$, and $w(x)$, results in a monotonic increase in $\Omega(x)$, i.e., a gradual increase in the degree of reinforcement from the base to the tip, which effectively resists the applied bending moment sketched in Fig. 9. We thus conclude that the wild bamboo geometry is optimized in the sense that every internode is endowed with an appropriate value of Ω .

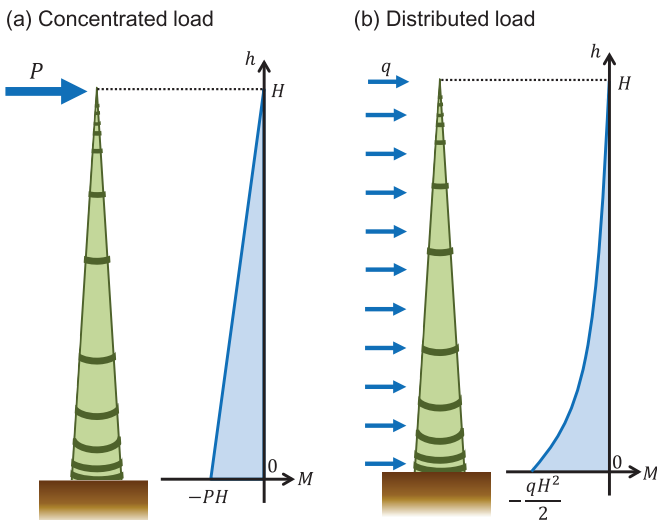
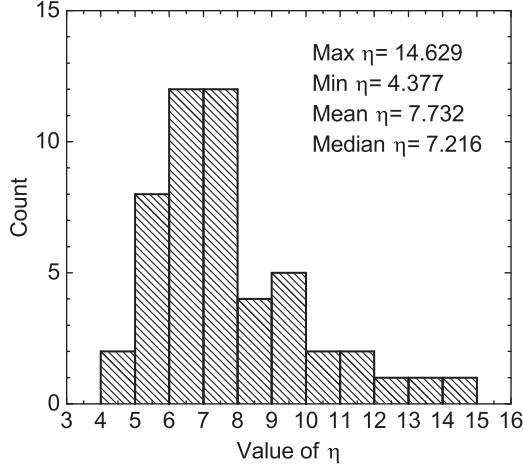


FIG. 9. Diagram of bending moment. (a) The case of a one-point concentrated load. (b) The case of a uniformly distributed load.

FIG. 10. Variation of η over 50 samples of wild bamboo culms.

V. CONCLUDING REMARKS

We have revealed the formula for optimal internode lengths in natural bamboo. Uneven internode lengths along the culm are key in assuring effective reinforcement based on a series of stiff diaphragms. Although our consideration has been restricted to a particular species (i.e., moso bamboo), the conclusion may apply to other species of bamboo as well. For instance, madake (*Phyllostachys bambusoides*) and hatiku (*Phyllostachys nigra*) were found to show similar profiles in $h(x)$ and $r(x)$ [46,47] as presented in Figs. 8(a) and 8(b). These imply a monotonic increase in $\Omega(x)$ and the presence of a small- x region in which the criterion of $\Omega < 2.033$ is satisfied in the same manner as in the case of moso bamboo. Quantitative comparison of the $\Omega(x)$ curves between different species of bamboo will be addressed in our future work.

It is also interesting to take into account the effect of spatial variation in E_{\parallel} and E_{\perp} across the woody part of the culm. Bamboo is, in principle, a functionally graded material in which the reinforcement fibers (i.e., vascular bundles and the bundle sheaths surrounding them) are distributed gradually in both the longitudinal and the radial directions [19,23]. The graduation may cause feasible variations in E_{\parallel} and E_{\perp} , suggesting a certain revision in the formulation of the strain energy U presented in Eqs. (5)–(7). We conjecture that a higher fiber density near the outer surface causes a further reduction in Ω since the dense fraction of fibers may facilitate the suppression of cross-sectional ovalization under a bending moment. To verify this conjecture in a quantitative manner, precise measurement of the anisotropic structural constants of bamboo and systematic microscopic observation of the fiber density would be of great help.

In conclusion, we have performed data analysis and theoretical considerations on the physical origin of nonuniform internode lengths in wild moso bamboo. Measurement-data-based computations of $\ell(x)$, $r(x)$, and $w(x)$ have revealed that the degree of ovalization suppression, quantified by $\Omega(x)$, is enhanced monotonically from the tip to the base of the culm. The monotonicity of the $\Omega(x)$ curve is in harmony with the degree of bending moment caused by the external load.

These results lead us to the conclusion that the wild bamboo's geometry is a consequence of self-adaptive control of $\Omega(x)$ under the restriction of the high-strength and lightweight principles. It is hoped that our results will shed light on novel biomimetic design of structurally optimized composite materials.

ACKNOWLEDGMENTS

We would like to thank an anonymous referee for valuable suggestions and critically reading of the manuscript. This work was supported by JSPS KAKENHI Grants No. 25390147, No. 26292088, and No. 15H04207. A.I. is grateful for the special grants from the president of the Prefectural University of Kumamoto (FY2008, FY2010, and FY2011).

APPENDIX A: DERIVATION OF EQ. (11)

In the situation shown in Fig. 5(e), the cylinder axis forms an arc of curvature radius R and arc length ℓ . Note that, at the center of that arc, the deviation from the horizontal line connecting the two centers of the disks at both edges is equal to $r\zeta$, i.e., the reduction in the minor axis of the cross section at the center of the short cylinder. Setting the angle ϕ as depicted in the figure, we have

$$R \cos \phi + r\zeta = R. \quad (\text{A1})$$

Since $\phi \ll 1$, or equivalently $R \gg \ell$, we have

$$r\zeta = R(1 - \cos \phi) = R \left(\frac{\phi^2}{2!} - \frac{\phi^4}{4!} + \dots \right). \quad (\text{A2})$$

We leave only the lowest order term in the expansion and use the geometric relation $\ell = R \cdot 2\phi$ to obtain

$$r\zeta \simeq \frac{\ell^2}{8R}. \quad (\text{A3})$$

As a result, the curvature κ of the arc is

$$\kappa = \frac{1}{R} \simeq \frac{8r\zeta}{\ell^2}. \quad (\text{A4})$$

APPENDIX B: EVALUATION OF η

The value of the parameter η , defined by Eq. (24), for moso bamboos was evaluated by the following procedure. Since there were no available data on either $r_{0,1}$ or ℓ , we deduced a new linear relation: $r_{0,1} = 0.466d_b + 0.231$ (coefficient of determination $R^2 = 0.997$), from statistical analysis of other existing data for the breast-height diameter d_b and $r_{0,1}$ over 200 samples [45]. It is noteworthy that d_b is a common dendrometric measurement, expressing the diameter of the trunk or bole of a standing tree at the height of an adult human's breast ($\simeq 1.3$ m) [49].

Figure 10 depicts the distribution of η for 50 samples of moso bamboos. The values range from 4.377 to 14.629, with the mean and median being 7.732 and 7.216, respectively. The Shapiro-Wilk normality test [50] indicates that η had a non-normal distribution ($P < 0.001$); we therefore employ the median of η in the present analysis.

- [1] L. Gratani, M. F. Crescente, L. Varone, G. Fabrini, and E. Digiulio, *Flora* **203**, 77 (2008).
- [2] N. N. Wai, H. Nanko, and K. Murakami, *Wood Sci. Technol.* **19**, 211 (1985).
- [3] U. Wegst, H. Shercliff, and M. Ashby, *The Structure and Properties of Bamboo as an Engineering Material* (University of Cambridge, Cambridge, UK, 1993).
- [4] K. Chung and W. Yu, *Eng. Struct.* **24**, 429 (2002).
- [5] W. Liese and M. Köhl, *Bamboo: The Plant and its Uses* (Springer, Berlin, 2015).
- [6] T. T. Veblen, F. M. Schlegel, and B. R. Escobar, *J. Ecol.* **68**, 397 (1980).
- [7] P. Shanmughavel and K. Francis, *Biomass Bioenerg.* **10**, 383 (1996).
- [8] J. Scurlock, D. Dayton, and B. Hames, *Biomass Bioenerg.* **19**, 229 (2000).
- [9] Y. Isagi, T. Kawahara, K. Kamo, and H. Ito, *Plant Ecol.* **130**, 41 (1997).
- [10] A. J. Nath, G. Das, and A. K. Das, *Biomass Bioenerg.* **33**, 1188 (2009).
- [11] A. J. Nath, G. Das, and A. K. Das, *For. Ecol. Manag.* **261**, 995 (2011).
- [12] S. Lakkad and J. Patel, *Fibre Sci. Technol.* **14**, 319 (1981).
- [13] J. J. A. Janssen, *Mechanical Properties of Bamboo* (Kluwer Academic, Dordrecht, Netherlands, 1991).
- [14] P. G. Dixon and L. J. Gibson, *J. R. Soc. Interface* **11**, 20140321 (2014).
- [15] L. Zou, H. Jin, W.-Y. Lu, and X. Li, *Mater. Sci. Eng. C* **29**, 1375 (2009).
- [16] S. Youssefian and N. Rahbar, *Sci. Rep.* **5**, 11116 (2015).
- [17] W. Liese, *The Anatomy of Bamboo Culms* (International Network for Bamboo and Rattan, Beijing, 1998).
- [18] F. Nogata and H. Takahashi, *Compos. Eng.* **5**, 743 (1995).
- [19] S. Amada, T. Munekata, Y. Nagase, Y. Ichikawa, A. Kirigai, and Y. Zhifei, *J. Compos. Mater.* **30**, 800 (1996).
- [20] T. Tan, N. Rahbar, S. M. Allameh, S. Kwofie, D. Dissmore, K. Ghavami, and W. O. Soboyejo, *Acta Biomater.* **7**, 3796 (2011).
- [21] J. J. García, C. Rangel, and K. Ghavami, *Constr. Build. Mater.* **31**, 52 (2012).
- [22] M. J. Richard and K. A. Harries, *Wood. Sci. Technol.* **49**, 99 (2015).
- [23] M. K. Habibi, A. T. Samaei, B. Gheshlaghi, J. Lu, and Y. Lu, *Acta Biomater.* **16**, 178 (2015).
- [24] S. P. Timoshenko and J. M. Gere, *Mechanics of Materials* (Van Nostrand Reinhold, New York, 1972).
- [25] K. Schulgasser and A. Witztum, *J. Theor. Biol.* **155**, 497 (1992).
- [26] H.-C. Spatz and T. Speck, *Biomimetics* **2**, 149 (1994).
- [27] S. Li, S. Fu, Q. Zeng, X. Zhao, and B. Zhou, *Biomimetics* **2**, 15 (1994).
- [28] Z. P. Shao, L. Zhou, Y. M. Liu, Z. M. Wu, and C. Arnaud, *J. Trop. For. Sci.* **22**, 133 (2010).
- [29] F. Wang, Z. Shao, Y. Wu, and D. Wu, *Wood. Sci. Technol.* **48**, 1257 (2014).
- [30] D. Taylor, B. Kinane, C. Sweeney, D. Sweetnam, P. O'Reilly, and K. Duan, *Wood. Sci. Technol.* **49**, 345 (2015).
- [31] K. Higuchi, *J. Jpn. For. Soc.* **63**, 379 (1981) (in Japanese).
- [32] A. Inoue, K. Kuraoka, and F. Kitahara, *J. For. Res.* **23**, 435 (2012).
- [33] L. G. Brazier, *Proc. R. Soc. London A* **116**, 104 (1927).
- [34] J. B. Keller, *Arch. Ration. Mech. Anal.* **5**, 275 (1960).
- [35] O. Fabian, *Int. J. Solid. Struct.* **13**, 1257 (1977).
- [36] A. P. Seyranian and O. G. Privalova, *Struct. Multidisc. Optim.* **25**, 393 (2003).
- [37] M. K. Wadee, M. A. Wadee, A. P. Bassom, and A. A. Aigner, *Proc. R. Soc. A* **462**, 817 (2006).
- [38] C. R. Calladine, *Theory of Shell Structures* (Cambridge University Press, UK, 1989).
- [39] H. Shima, M. Sato, and S.-J. Park, *Adv. Condens. Matter Phys.* **2014**, 923896 (2014).
- [40] S. Amada, Y. Ichikawa, T. Munekata, Y. Nagase, and H. Shimizu, *Compos. Part B* **28**, 13 (1997).
- [41] U. G. K. Wegst and M. F. Ashby, *J. Mater. Sci.* **42**, 9005 (2007).
- [42] M. K. Habibi and Y. Lu, *Sci. Rep.* **4**, 5598 (2014).
- [43] A. Inoue, F. Kitahara, H. Suga, and T. Wajima, *Landscape Ecol. Eng.* **7**, 153 (2011).
- [44] M. Kunze, *Suppl. Tharander Forstlich. Jahrbuche* **2**, 1 (1881).
- [45] H. Suga, A. Inoue, and F. Kitahara, *J. For. Res.* **16**, 261 (2011).
- [46] A. Inoue, S. Sakamoto, H. Suga, and F. Kitahara, *Biomass Bioenerg.* **35**, 2666 (2011).
- [47] A. Inoue, S. Sakamoto, H. Kitazato, and K. Sakuta, *J. For. Plann.* **18**, 13 (2012).
- [48] L. Rui, M. J. A. Werger, H. J. During, and Z. C. Zhong, *Flora* **194**, 89 (1999).
- [49] P. W. West, *Tree and Forest Measurement* (Springer-Verlag, Berlin, 2009).
- [50] S. S. Shapiro and M. B. Wilk, *Biometrika* **52**, 591 (1965).